

A Diagnostic Technique for Targeting during Airborne Seeding Experiments in Wintertime Storms over the Sierra Nevada

ROBERT M. RAUBER

Electronic Techniques, Inc., Ft. Collins, Colorado

ROBERT D. ELLIOTT

North American Weather Consultants, Salt Lake City, Utah

J. OWEN RHEA

Auburn, CA 95603

ARLEN W. HUGGINS*

Electronic Techniques, Inc., Ft. Collins, Colorado

DAVID W. REYNOLDS

U.S. Bureau of Reclamation, Auburn, California

(Manuscript received 15 August 1987, in final form 24 November 1987)

ABSTRACT

A diagnostic technique for targeting during airborne seeding experiments has been developed for the Sierra Cooperative Pilot Project (SCPP). This technique was used operationally during SCPP for real-time guidance to aircraft, providing 1) the location and orientation of the seeding line required to target ice particles created by seeding to a specified ground location and 2) an estimate of the areal coverage of the seeding effect on the ground. Procedures to use this technique as a real-time guidance tool during seeding operations in Sierra wintertime storms are discussed.

Three evaluation studies of the targeting method are presented. These include 1) comparisons of diagnosed wind fields with those measured by aircraft; 2) comparisons of ice particle growth rates and habits within seeded cloud regions with those used in the targeting computations; and 3) comparison of radar echo evolution within seeded cloud regions with calculated particle trajectories.

1. Introduction

The Sierra Cooperative Pilot Project (SCPP) was initiated by the U.S. Bureau of Reclamation in the early 1970s to study the wintertime meteorology of the Sierra Nevada, to identify conditions when cloud seeding may cause changes in precipitation from wintertime Sierra storms and to estimate the magnitude of those changes (Reynolds and Dennis 1986). A specific purpose of the SCPP was to develop new technology to better identify seeding opportunities and appropriately direct seeding efforts within Sierra Nevada river basins.

* Present affiliation: Desert Research Institute, Atmospheric Science Center, Reno, NV 89506.

Corresponding author address: Dr. Robert M. Rauber, Dept. of Atmospheric Sciences, University of Illinois, 102 Atmospheric Sciences Building, 105 South Gregory Ave., Urbana, IL 61801.

A substantial effort was made in the SCPP to develop a simple technique that could be used operationally to target seeding effects during aircraft seeding experiments. The purpose of this article is to describe this technique and to discuss its utility in wintertime cloud systems over the central Sierra Nevada.

2. SCPP Fixed Target Experiment

The Sierra Cooperative Pilot Project has been reviewed recently by Reynolds and Dennis (1986). The SCPP operated within the American River Basin (ARB) of the central Sierra. Figure 1 shows the location of the major measurement systems within the ARB and the topography of the region. SCPP aircraft, remote sensing, and ground based instrumentation systems, including all those used in this paper, have been discussed by Huggins and Rodi (1985), Humphries (1985), Gordon and Marwitz (1986), Reynolds and Dennis (1986), Heggli et al. (1987), and Marwitz (1987).

Beginning in 1984/85, SSCP initiated a randomized exploratory fixed target experiment (Flueck 1982) to test the effects of aerial seeding on precipitation enhancement from orographic clouds. The target was designated as a 750 km² area above 1.5 km elevation in the northeast corner of the ARB (see Fig. 1). The purpose of this experiment was to observe, as completely as possible, the chain of events leading from nucleation to precipitation for particles created by seeding within the orographic clouds. Preliminary results of this experiment have been discussed by Martner (1986) and Deshler and Reynolds (1987).

Targeting seeding effects within the fixed target area was critical to experiment evaluation. For SSCP, targeting was particularly important, since the ground-based microphysical observations were limited to one location at Kingvale (Fig. 1). Targeting required a technique that could 1) accurately reproduce the major characteristics of the airflow across the mountain within the seeded region of the cloud; 2) closely reproduce the growth and fallout trajectories of ice particles created by seeding; 3) predict the location where aircraft should seed to produce effects at the target; 4) account for dispersion of a seeding curtain by vertical wind shear and particle fall velocity spectra variations (see Stewart and Marwitz 1982a); 5) be initialized with typical data available to the program; and 6) run in real time.

The problem of targeting was complicated by the complex structure and rapid changes that characterize Sierra Nevada winter storms. Many storm systems that pass over the Sierra Nevada were found to have similar features to those observed over the Pacific Northwest (Hobbs 1978) and the British Isles (Browning and

Monk 1982). During such storms, cloud systems often evolved in a sequence similar to that shown in Fig. 2 (Reynolds and Dennis 1986). Maximum supercooled liquid water content (and, by inference, maximum precipitation enhancement potential) was often found to occur following the passage of the upper-level cold front as the cloud top lowered (Heggli and Reynolds 1985; Reynolds and Kuciauskas 1987). During this phase of the storm, winds at cloud level generally changed continually with time in response to the passage of mesoscale and synoptic scale features. In many storms, a low-level barrier jet was present (Parish 1982). The speed of this jet, and its horizontal and vertical extent, varied from storm to storm.

Calculating accurate wind fields over the Sierra Nevada in a time frame useful for targeting calculations proved to be difficult. During the years of the fixed target experiment (1984/85 through 1986/87), SSCP scientists experimented with simple parameterizations of the airflow (Elliott 1981; Elliott and Rhea 1984; Rhea and Elliott 1986), detailed simulations using the model of Anthes and Warner (1978) as adapted by Parish (1982) and Waight (1984), and detailed more complex simulations using the nested grid model of Clark (1977) (Smolarkiewicz et al., unpublished). The latter models proved valuable for research, but no method could consistently reproduce accurate wind fields within the seeded cloud region in a time frame necessary for an airborne seeding experiment. Two basic problems hampered progress in solving the targeting problem:

- 1) Sierra Nevada storms often contain mesoscale features with horizontal scales on the order of the

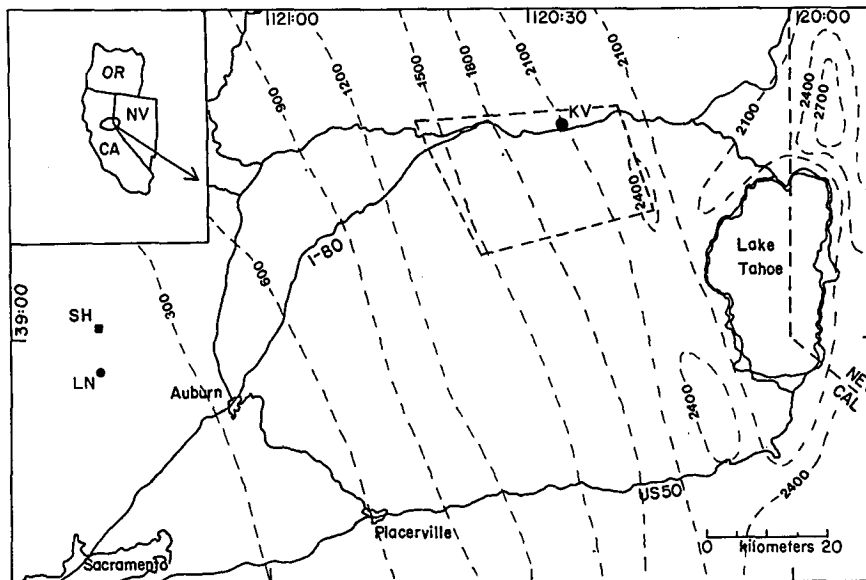


FIG. 1. Map of the SSCP research area showing the location of the area in California, the location of the Lincoln, Sheridan and Kingvale rawinsonde launch sites, the mean topography of the region, and the target area (dashed box) for the fixed target seeding experiment.

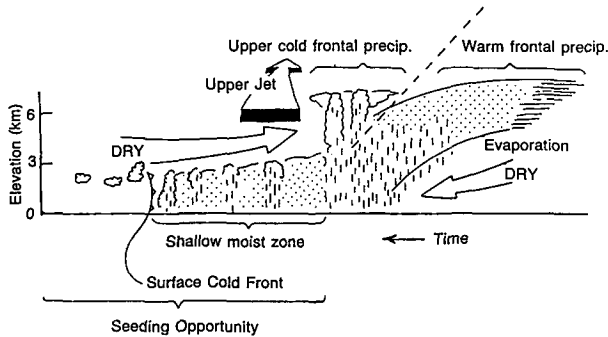


FIG. 2. Conceptual model of a cross section through many Sierran storms. Stippled areas denote relative humidities above 90%. Most seedable regions determined from radiometric and aircraft observations are annotated. The time of passage of a complete storm can vary significantly from as short as 12 to >48 h (from Reynolds and Dennis 1986).

mountain width (~100 km). These features were not well represented by a single vertical sounding at the base of the mountain normally used to initialize models.

2) Sierra Nevada storms were seldom, if ever, steady state. Wind fields over the Sierra Nevada continually changed in storms in response to the storm's mesoscale and synoptic scale evolution. Significant changes often were observed in time scales as short as 3 h.

By the 1984/85 season, it was recognized that simultaneous rawinsondes were required at least every 3 h at two sites, one near the base of the Sierra Nevada Range and one near the Sierra Nevada Crest to monitor changes in the wind fields associated with mesosynoptic-scale storm evolution. The valley launch sites were either at Sheridan, California (60 m MSL, collocated with the radar) or Lincoln, California (57 m MSL, 1986–87 season only). The high elevation launch site was at Kingvale (1800 m MSL), which was collocated with the ground microphysical measurements and within the fixed target area. These soundings provided measurements of the wind fields at the boundaries of the seeded volume at a frequency necessary to resolve changes due to the passage of synoptic-scale and mesoscale features. Additional soundings were provided by the research aircraft during takeoff over the valley and by supplemental soundings launched at Kingvale. The dual-sounding system was incorporated operationally for targeting in SCPP beginning in February 1986.

In this paper, the diagnostic technique developed to guide aircraft to the appropriate location to target seeding effects within the ARB using this dual-sounding system is described. Evaluations of the parameterizations used to recover the wind fields across the Sierra Nevada and simulate ice particle growth are presented. Finally, we present a case study comparing radar echo evolution within a seeded cloud region with predicted particle trajectories.

3. Targeting methodology

In this section, we describe the components of the targeting method used during the last 2 yr of SCPP. This targeting method was designed for operational expediency. The program was developed for use on a minicomputer, but can operate on a personal computer. The total time required to run the program on either system and relay information to the aircraft was usually under 3 min. Rawinsonde data used in the computations were normally available from the field within 30 min after the termination of the sounding. Aircraft and radiometer data were available in real time. The methods presented here focus only on the multiple-rawinsonde technique that was utilized successfully later in the program.

a. Kinematics

Wind speed and direction were measured in vertical soundings at two locations, Sheridan or Lincoln, in the Sacramento Valley, and Kingvale, near the Sierra Crest. These sites were separated by 85 km. Seeding was normally conducted at or below the 3500 m level (~650 mb). The "target" in all cases was Kingvale.

The primary region where accurate winds were required for targeting, designated as region A on Fig. 3, was bounded on the west by Sheridan, the east by Kingvale and aloft approximately by 650 mb (surface "D" on Fig. 3). Regions B, downwind of the crest, and C, in the upper troposphere, were normally outside the primary region of interest during airborne seeding experiments. However, it was possible that particle trajectories occasionally would fall into region B (trajectory 2 on Fig. 3) or initiate or pass briefly into the lower part of region C (trajectory 3 on Fig. 3).

The procedure to determine winds in each region differed because of data availability. In region A, the primary region of interest for the experiment, winds were determined in the following way:

The barrier-perpendicular (u) component was determined by assuming conservation of mass flux throughout the domain A. The mass flux perpendicular to the crestline below the 650 mb level at Sheridan was measured directly from the sounding by calculating

$$M_s = g^{-1} \int_{P_{sh}}^{P_{650}} u(P) dp. \quad (1)$$

Here, M_s is the mass flux below 650 mb at Sheridan, P pressure, g gravity, and the subscripts sh and 650 denote the surface pressure and the 650 mb pressure at Sheridan. A similar integration was then performed at Kingvale to determine the pressure level over Kingvale where the mass flux at Kingvale, M_k , equaled M_s :

$$M_s = M_k = g^{-1} \int_{P_{kv}}^{P_i} u(P) dp. \quad (2)$$

Here P_i is the pressure level at Kingvale below which $M_k = M_s$, and P_{kv} is the surface pressure at Kingvale.

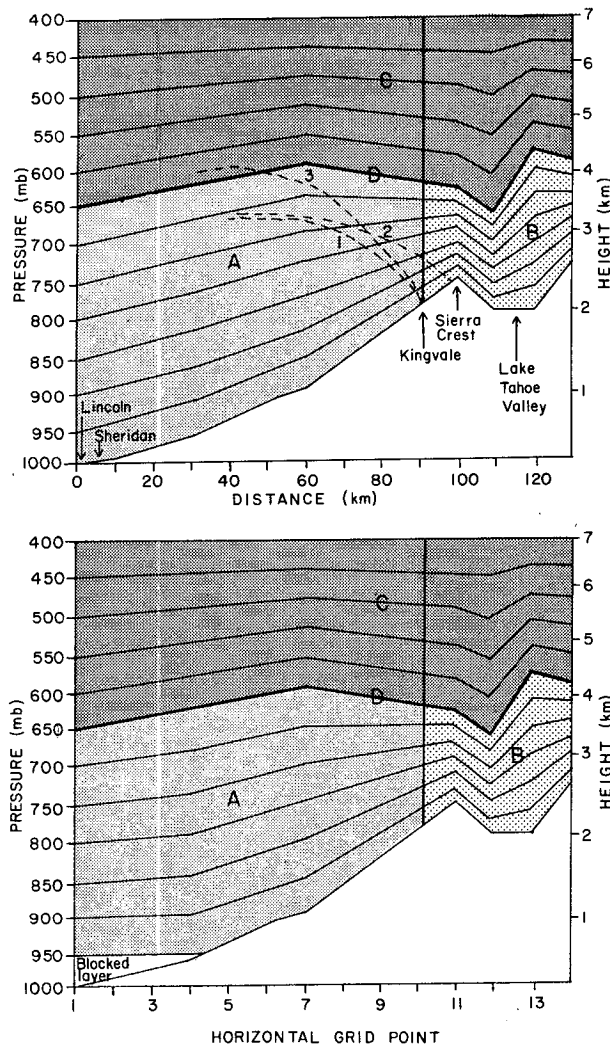


FIG. 3. Flow channel configuration used to determine wind components without (top) and with (bottom) the presence of a blocked surface layer. Regions A–C and surface D are discussed in the text. The coordinate system was aligned with the Sierra Nevada crestline and chosen so that the Sierra Crest was located 100 km from the origin. Sheridan was located 7 km east of the origin and Lincoln at the origin. Both soundings were assumed to apply at the origin since they were located well within the Sacramento Valley.

These two points, P_{650} and P_t , were then connected by a surface, defined in Fig. 3 as the surface D. The profile of this surface was assumed to have a peak 40 km upwind of the crest. This profile was chosen instead of a linear profile to characterize the upstream propagation of the primary mountain wave predicted by theories of mountain airflow (e.g., Smith 1979). The mean position of the airflow crest during meteorological conditions typical of fixed target experiments was determined by examining 1) aircraft measurements of equivalent potential temperature (θ_e) between the base of the Sierra Nevada and the crestline; 2) θ_e analyses constructed from data collected by simultaneously released rawinsondes at Sheridan, Kingvale, and a middle

elevation site (1600 m), Blue Canyon; and 3) numerical simulations of the cross-barrier airflow using the two-dimensional primitive equation airflow model for Sierra Nevada terrain developed by Parish (1982) and Waight (1984).

Surface D and the terrain below define a large channel of air flowing between Sheridan and Kingvale. Within this channel, mass flux was assumed to be conserved. This large channel of air was then subdivided into seven smaller channels of equal pressure depth (50 mb at the inflow location). The u -component in each individual channel was then determined by assuming mass flux conservation within each smaller channel, such that

$$u_{i,j} = u_{i,1}(\Delta P_{i,1})(\Delta P_{i,j})^{-1} \quad (3)$$

where $u_{i,1}$ = u -component in flow channel i at inflow boundary, $u_{i,j}$ = u -component in flow channel i at downward grid point j (10 km spacing), $\Delta P_{i,1}$ = depth of flow channel i at inflow boundary (50 mb), and $\Delta P_{i,j}$ = depth of flow channel i at downwind grid point j . On occasion, a blocked surface layer ($u < 2.5 \text{ m s}^{-1}$) was present within the Sacramento Valley. When such blocked flow conditions existed in the lowest levels, the integration (Eq. 1) began at the top of the blocked layer rather than at P_{sh} . The profile of the terrain surface was then adjusted to incorporate the region of blocked flow (Fig. 3b).

Vertical motion was determined by computing

$$w = u(\Delta h/\Delta x) \quad (4)$$

where $\Delta h/\Delta x$ is the slope of the flow channel between grid points. Typical vertical velocities varied from 0.1 m s^{-1} over the lower foothills to 0.5 m s^{-1} near the crestline. The barrier-parallel (v) component was determined by direct interpolation along the flow channels of the v -component measured at Sheridan and Kingvale. Derivatives of all variables in the y (barrier parallel) direction over the research area were assumed to be zero.

Region B on Fig. 3, which included the Lake Tahoe valley downwind of the crest, had no measurement support to calculate wind fields. Winds in this region were estimated by assuming a profile of surface D which corresponded approximately to the terrain shape. The profile of surface D downwind of the crestline was also adjusted to account for the upstream vertical propagation of the mountain wave associated with the mountain range east of Lake Tahoe (see Fig. 3). The u - and w -components of the wind in region B were then determined by the methods described above. The v -component was conserved in each flow channel downwind of the crest.

Winds in region C were estimated by assuming mass conservation between surface D and the 400 mb surface. Since the 400 mb surface was assumed to be horizontal, this assumption artificially accelerated winds near the top of region C in the vicinity of the mountain

crest. These accelerations had no effect on any of the trajectory calculations. The trajectories that did pass into region C did so only in the lower regions well upwind of the crestline (see Fig. 3). To estimate the wind components in region C, the region was divided into five additional flow channels of equal pressure depth. The u -, v -, and w -components of the flow were then calculated in a manner similar to regions A and B.

The method to determine the wind fields for targeting applies to flow in a stable or neutral atmosphere. In many storms, convective motions were also present. In conditions typical of fixed target experiments, weak convection often occurred, generally embedded in the larger-scale orographic cloud. The depth, frequency, duration and strength of these convective motions were functions of the time and location in the storm and were, in general, unpredictable.

An estimate of the possible errors that convective motions may introduce to targeting calculations has been calculated by King (1984). King studied the effects of several cloud parameters on targeting in stratiform clouds containing weak embedded convection that occur over western Victoria, Australia. He found that varying the magnitude of a constant updraft in his targeting calculations from 0.0 to 0.5 m s^{-1} , all other variables staying the same, caused an overall 16% change in the transit time of a particle from its nucleation point to the surface. In SCPP clouds, the mean vertical velocity due to orographic lift encountered by a particle, based on the terrain slope and typical horizontal velocities, was in the range 0.2–0.4 m s^{-1} . Convective motions, positive or negative, could impose on these orographic motions brief periods of vertical velocities exceeding 1 m s^{-1} . Averaged over the total particle trajectory, the mean vertical velocity including convection would most likely fall within the range of $\pm 0.5 \text{ m s}^{-1}$ of the value for pure orographic flow. Using King's estimates, it is probable that convection could cause errors in the total transit time up to 16%. The corresponding displacement of the impact point would depend on the intensity and location of the convection when encountered by the particle and the horizontal wind speeds. In SCPP experiments, it was likely that the variations in seeded particle trajectories imposed by convection were averaged out by seeding over a sufficiently long time period with several seedlines. Typical experiments continued for 1–2 h with five–ten seedlines placed within the clouds.

b. Microphysics

1) PARTICLE GROWTH RATES AND HABITS

Ice crystal habits and particle axial growth rates are highly dependent on temperature and supersaturation (Hallett and Mason 1958; Kobayashi 1961; Magono and Lee 1966; Ryan et al. 1976). Because seeding oc-

curred at a variety of cloud temperatures, a critical aspect of targeting was to determine fall velocity as a function of particle habit and size. Accurate targeting required a reasonable estimate of ice particle growth rates and fall velocities.

The parameterization developed for targeting during SCPP operations used the linear growth rates for the basal (c) and planar (a) crystal axes specified by measurements of Ryan et al. (1976). They found crystal axial growth rates to be maximum along the a -axis at -17°C and maximum along the c -axis at -6°C . A distinct minimum in growth rate along both axes occurred at -10°C . Axial growth rates measured by them were incorporated in the targeting calculations. The measured growth rates extend through the first few minutes of crystal growth. However, measurements of Fukuta and Wang (1984) extend up to 20 min. Fukuta and Wang's data suggest that the linear growth rates reported by Ryan et al. apply at times as long as 20 min. Crystal habits were determined on the basis of temperature and crystal axial ratios. The algorithm is discussed in following sections.

2) CLOUD LIQUID WATER AND RIMING

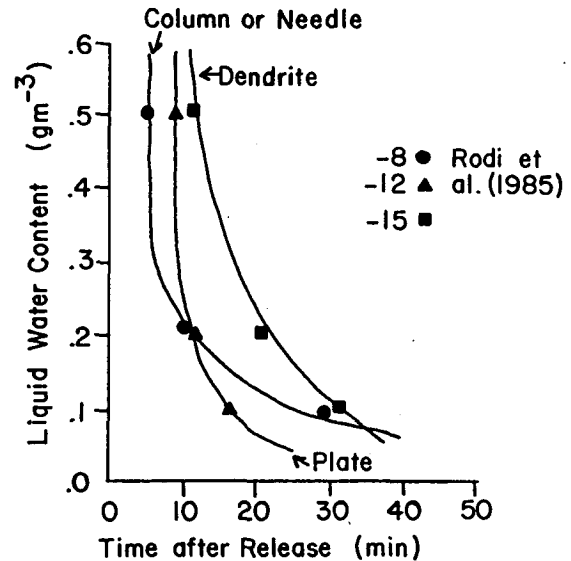
The importance of accurately specifying the liquid water content of a cloud when calculating particle trajectories during seeding operations has been demonstrated by King (1984). He showed, using model calculations within stratiform clouds, that the trajectories of cloud and precipitation particles growing by riming depend primarily on liquid water content, and not on the precise details of cloud temperature, crystalline shape, graupel shape or size. Unfortunately, in natural clouds, the liquid water content and distribution of liquid are unknown and generally variable in time. During SCPP, two measurements of liquid water content were available on a real time basis, the first from aircraft and the second from a ground-based radiometer. The relationship between liquid water depth measured by the radiometer and actual cloud liquid water content depends on the depth and distribution of liquid-bearing cloud layers. A climatological analysis of SCPP radiometric measurements by Heggli (1986) suggested that liquid was confined primarily to the lowest 1–2 km layer of cloud. An approximation of the average cloud liquid water content was obtained operationally by assuming that the liquid water was distributed uniformly over a kilometer-deep layer above the radiometer. The average liquid water content of the cloud (g m^{-3}) would then be numerically equal to the liquid water depth measured by the radiometer (millimeters).

Aircraft measurements of liquid water content were made at the minimum obstruction clearance altitude (MOCA) on a descent westward from the crestline to approximately the melting level. Measurements were

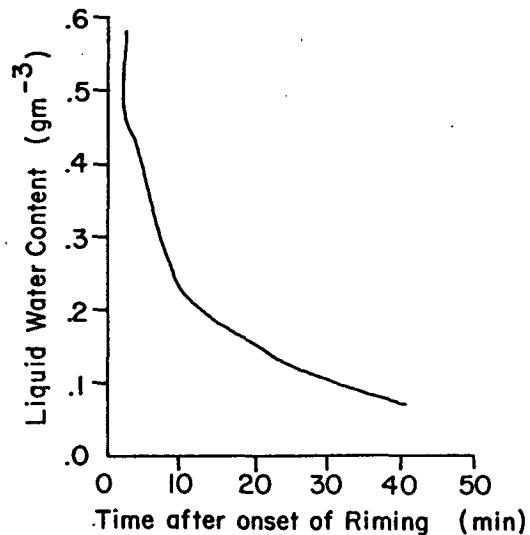
also made along the seedline prior to seeding. The MOCA in the Sierra region is approximately 300 m above the terrain. The radiometric and aircraft measurements were both considered when estimating the average cloud liquid water content. The value of liquid water content used in the targeting calculations was chosen subjectively based on the values measured by the radiometer and aircraft, and on the upward or downward trend of the radiometric measurements. Operationally, the goal was to reasonably anticipate the cloud liquid water content during the seeding experiment. The liquid water content assigned as an input variable in the targeting calculation was assumed to characterize the entire cloud system along the particle trajectories.

Several studies have considered the riming process with particular application to the Sierra Range (Reinking 1974, 1979; Rodi et al. 1985; Prasad 1986). Reinking's data provide information concerning the minimum crystal size necessary for onset of riming, but provide no information concerning the effect of variations in average liquid water content of the cloud. Rodi et al. (1985) and Prasad (1986) used a microphysical model developed by Heymsfield (1982) and Heymsfield and Pflaum (1985) to estimate the onset of riming in Sierra fixed-target type cloud systems. Their studies specified the time of onset of riming as a function of liquid water content and cloud temperature. Figure 4 shows the onset time of riming as a function of liquid water content for three temperatures specified by Rodi et al. (1985). The lines are visual fits to these data points for extrapolation to other liquid water contents. In the parameterization used in SCPP, these curves were assumed to apply for dendritic habits (-15°C , squares), plates (-12°C , triangles), and columns or needles (-8°C , circles). This parameterization allowed an estimate of the time of riming onset on the basis of two measurable parameters, cloud liquid water content and temperature.

Once the onset of riming occurred, the particle was assumed to encounter supercooled water throughout the remainder of its trajectory. A uniform distribution of liquid along the trajectory was assumed. The rate at which a particle becomes rimed is a function of liquid water content. The time after onset of riming that a particle became heavily rimed was assumed to be a function of the cloud liquid water content. The parameterization used is shown on Fig. 4. The rate of conversion was relatively slow (40 min) at minimal liquid water content ($<0.10\text{ g m}^{-3}$), but proceeded quickly at high liquid water content ($0.30\text{--}0.50\text{ g m}^{-3}$). Typically, in fixed target experiments, the measured liquid water content was $0.05\text{--}0.20\text{ g m}^{-3}$. Based on past data collected on the frequency of supercooled water, target crystals in most fixed-target conditions would become heavily rimed within 15–25 min after onset, although in very wet conditions, heavy riming could occur in as short as 2 min (see section 4).



(a)



(b)

FIG. 4. (a) Onset time of riming as a function of liquid water content. (b) Time after riming onset that an ice particle is assumed to be heavily rimed.

3) PARTICLE FALL VELOCITIES

Fall velocities of ice particles are a strong function of particle shape, mass and degree of rime. Studies of particle fall velocity can be broadly divided into two types: 1) theoretical studies using relationships between the Best and Reynolds numbers (Cornford 1965; List and Schemenauer 1971; Kajikawa 1971); and 2) direct measurements of ice particle fall velocities using stroboscopic methods (Brown 1970; Davis 1974; Locatelli and Hobbs 1974). Our approach was to use the direct measurements of Brown (1970), Davis (1974), and Lo-

catelli and Hobbs (1974). Four particle habits were considered. Two equations were used for each particle, the first for an unrimed particle and the second for a heavily rimed particle. A smooth transition between equations was used as the particles grew, based on the time of onset of riming and time of heavy rime coverage (see Eqs. 5 and 6 below). The fall velocity equations for each habit class are summarized in Table 1.

In Table 1, V_t is the particle terminal velocity (meters per second) and c or a is the particle major axis (centimeters). For dendrites, it was assumed that it would become heavily rimed but recognizable when rime completely covered the particle (see Locatelli and Hobbs 1974). Plates were assumed to rime into spherical shape and become graupel. The available equations for columns have opposite inflections (see Fig. 5) with common points at 0 and 0.09 cm. At sizes smaller than 0.09 cm, the equation of Davis (1974) was used for unrimed particles while Locatelli and Hobbs (1974) was used for rimed particles. At sizes ≥ 0.09 cm, the equation of Locatelli and Hobbs was used independent of rime coverage. Locatelli and Hobbs reported that the maximum dimension of columns was near 0.2 cm. The fall velocity of a column of length 0.2 cm was considered as the upper fall velocity limit. Columns with length > 0.2 cm were assumed to fall at the rate of a column with length equal to 0.2 cm. The equations for unrimed needles are linear fits to the data of Nakaya (1954) and Brown (1970) for three size ranges. As with columns, a maximum velocity limit was imposed. However, this maximum velocity corresponded to a larger size particle (0.35 cm) since needles are often observed to be larger than 0.2 cm. We were unable to find any studies in the literature which provided measurements of the fall velocity of rimed needles. To simulate their fall velocity, it was assumed that these particles achieved a fall velocity equal to $1.5V_{tn}$, where V_{tn} is the fall velocity of the unrimed single needle.

4) PARTICLE GROWTH REGIMES

An ice crystal experiences a wide range of conditions during its transit from nucleation to impact with the

ground. For targeting purposes, these conditions were parameterized into four growth stages. During the first stage, which extended from the time of nucleation to 300 s, particle diffusional growth was allowed to proceed independently along the a and c axes. Riming was not permitted. A 60 s time step was used. This time step was found to be sufficient to resolve small changes in particle fall velocity and changes in environmental winds along the trajectory. The fall velocity of the particle was that of an unrimed plate (a axis $>$ c axis) or column (c axis $>$ a axis). At the end of 300 s, the habit was established. The particle was assumed to retain this habit throughout its trajectory. The habit criteria at 300 s growth was as follows:

Temperature (°C)	Axis	Particle type
≤ -13	a axis $\geq c$ axis	dendrite
> -13	a axis $\geq c$ axis	plate
< -6	c axis $>$ a axis	column
≥ -6	c axis $>$ a axis	needle

During the second growth stage, from 300 s to onset of riming, particle diffusional growth continued. Riming was not permitted. The fall velocity was that of the appropriate habit.

The third stage extended from onset of riming to heavy rime coverage. The particle growth continued at a rate specified by the diffusional growth rate. In addition, a smooth transition between the fall velocity for the unrimed and rimed particles of the form

$$V_t = AV_{tr} + (1 - A)V_{tu} \tag{5}$$

was employed. Here,

$$A = (t - t_o)/(t_r - t_o) \tag{6}$$

where t is the current time, t_o the time of onset of riming, t_r the time when heavy rime coverage developed, V_{tr} the fall velocity of the rimed particle and V_{tu} the fall velocity of the unrimed particle.

TABLE 1. Fall velocity (V_t , m s⁻¹) equations as a function of crystal major axis (centimeters) used in SCPP targeting calculations.

Type	Equation	Reference
1. Dendrite, unrimed	$V_t = 0.6197a^{0.217}$	Brown (1970)
Dendrite, rimed	$V_t = 1.32a^{0.330}$	Locatelli and Hobbs (1974)
2. Plate, unrimed	$V_t = 2.96a^{0.824}$	Davis (1974)
Graupel	$V_t = 3.34a^{0.460}$	Locatelli and Hobbs (1974)
3. Column unrimed ($c < 0.09$ cm)	$V_t = 24.3c^{1.309}$	Davis (1974)
Column unrimed ($c > 0.09$ cm)	$V_t = 3.99c^{0.56}$	Locatelli and Hobbs (1974)
Column rimed	$V_t = 3.99c^{0.56}$	Locatelli and Hobbs (1974)
Column ($c > 0.2$ cm)	$V_t = 1.62$	Locatelli and Hobbs (1974)
4. Needles unrimed ($0 < c < 0.1$ cm)	$V_t = 5c$	Brown (1970), Nakaya (1954)
Needles unrimed ($0.1 < c < 0.2$ cm)	$V_t = 2.1c + 0.29$	Brown (1970), Nakaya (1954)
Needles unrimed ($0.2 < c < 0.35$ cm)	$V_t = 1.2c + 0.47$	Brown (1970), Nakaya (1954)
Needles unrimed ($c > 0.35$ cm)	$V_t = 0.89$	
Needles (rimed or aggregated)	$V_t = 1.5V_{t(\text{unrimed})}$	

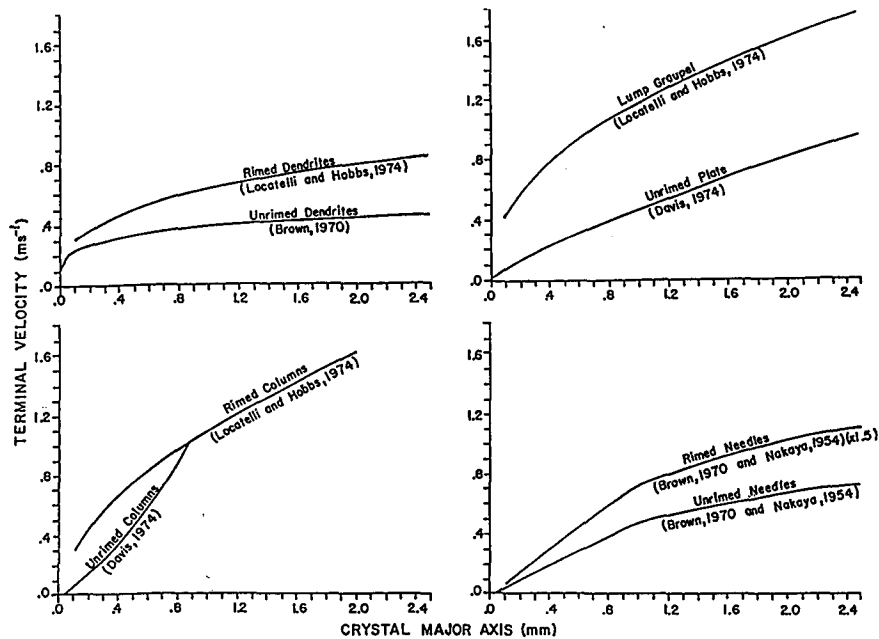


FIG. 5. Terminal velocity function for an (a) unrimed and rimed dendrite, (b) unrimed plate and lump graupel, (c) unrimed and rimed column, and (d) unrimed and rimed needle from Locatelli and Hobbs (1974), Davis (1974), Brown (1970) and Nakaya (1954).

The final growth stage extended from the time when heavy rime coverage first occurred to impact with the ground. The particle growth along the major axis continued at a rate specified by the diffusional growth rate. The particle fell as a rimed particle. The terminal velocity parameterizations for each of the four habit classifications are shown in Fig. 5.

The simple approach, discussed above, neglects important aspects of crystal growth and fallout in the interest of operational utility. First, the assumption of water saturated conditions throughout the cloud system can be incorrect. Evidence from aircraft measurements show that most cloud systems are inhomogeneous with saturated and subsaturated regions somewhat randomly distributed within the cloud. In addition, over-seeding water saturated clouds has the potential to reduce the saturation level to below water saturation because of competitive growth between large numbers of ice particles. In general, the assumption of water saturated conditions throughout the cloud system will result in an overall overestimation of the ice particle growth rates. A second factor not accounted for in the parameterization is the pressure dependence of the diffusivity of water vapor in air. Alone, this would result in an underestimation of ice particle growth rates, particularly at high altitudes. The dependence of the fall velocity on the density and dynamic viscosity of air and on the Reynolds number (R) is also not accounted for in the parameterization. Typical particles observed by aircraft in seeded regions had $R < 50$. Underestimations in fall velocity from 2%–13% were possible due to this simplification for atmospheric conditions

characterizing the seeding experiments. Aggregation and ice multiplication were not considered in the trajectory calculations. Aggregation was not considered because the process was seldom observed in any aircraft or ground based observations of seeding effects in fixed target type cloud systems (e.g., Martner 1986; Deshler and Reynolds 1987). However, it should be noted that aggregation was important in purely convective clouds (Huggins and Rodi 1985). Ice multiplication was not included because the process would have little effect on the trajectory of the target crystal although it could affect the final distribution of precipitation.

c. Seeding techniques

Aircraft generally employed one of three seeding methods; dry ice (CO_2), droppable pyrotechnics (AgI), or airborne acetone generators (AgI). During the SCPP, all of the methods were utilized and tested to the extent possible. Choosing the appropriate location in the cloud to seed for each method, and the appropriate time to sample precipitation to identify seeding effects was fundamental to the experiment's success. The procedures incorporated into targeting computations to address each of these seeding strategies are discussed in this section.

1) LOGISTICAL PROCEDURES

Aircraft seeding involved a highly interactive process between the ground based forecaster, who initiated and interpreted targeting guidance and other meteorological data, and the seeder and research aircraft crews, who

falling seeding material curtain and was the altitude typically flown by the research aircraft. Referring to Fig. 6, a first estimate of the particle trajectory (line AB) was calculated. The error in this trajectory was calculated by determining the direction and distance between the impact point and the target (vector BD). The first estimate of the SLCP (point C) was determined by moving from the origin the direction and length of BD. This procedure was repeated again using point C as the new starting point. More than one iteration was required because the particle moved through a different region of the wind field in each iteration. The procedure continued iteratively until the solution converged on the SLCP. Normally, convergence to within 1 km of the target occurred after three iterations. Once the SLCP was calculated, the seedline orientation and length were determined. The seedline was oriented perpendicular to the line connecting the SLCP and the target. For research purposes in SCPP, the length of the seedline was varied with distance from the target (see Table 2). To maximize seeding effects over a small target area at the ground, it was desirable to seed as much of the volume of air as possible by making the seedlines shorter and closer together. However, errors in the calculated wind direction have a greater potential to cause particles created by seeding to miss the target when the seedlines are short. The length of the seedlines were calculated by assuming a $\pm 20^\circ$ error in the calculated wind direction. As the trajectories of particles became longer due to higher wind speeds, the length of the seedlines were increased proportionally. The values appearing in Table 2 were chosen to satisfy the 20° error criterion and operational requirements of the aircraft. Once the SLCP and seedline were known, a final trajectory was calculated for a crystal originating at the SLCP. The predicted crystal habit, rime characteristics, fall velocity evolution and total fall time were recorded for later analysis.

The areal coverage of the seeding effect at the ground is a function of the depth the seeding material falls in the atmosphere, the vertical wind shear within that depth, the variations in fall velocity that develop as crystals originating near the same location encounter differences in saturation and liquid water content along their trajectories, and, in the case of AgI, variation in the activation time of individual AgI aerosol (see Rhea and Elliott, 1986). For CO₂ and pyrotechnic seeding, all effects except AgI activation were considered.

TABLE 2. Seedline length versus trajectory length (T).
SCPP fixed target experiments.

Trajectory length (T) (km)	Seeding line length [km (nmi)]
$T < 10$	10 (5)
$30 > T \geq 10$	19 (10)
$45 > T \geq 30$	28 (15)
$T \geq 45$	37 (20)

Stewart and Marwitz (1982a) discuss in detail the mechanism of spreading of an initially vertical column of ice crystals due to vertical shear and variation in particle fallspeed. Unfortunately, the variations in particle fall velocity that occur in a sample of ice particles due to variations in particle growth rates have not been determined quantitatively. Variations in particle velocity were parameterized by allowing five particles to fall from each level. The fall velocity of each of these particles was given by

$$V_{in} = 0.1(n + 6)V_t, \quad n = 1, 2, 3, 4, 5 \quad (7)$$

where V_{in} is the fall velocity of particle n and V_t is the standard terminal velocity calculated from the equations in Table 1.

The depth of the seeding curtain varied with the type of flare used or the mean diameter of the CO₂ pellets. In SCPP, extensive tests were conducted prior to each field experiment to determine the depth that flares fell while burning and CO₂ pellets fell before sublimating. The flares (TB1-20 g flares)¹ consistently fell about 1000 m. The size of CO₂ pellets varied from year to year depending on the dispensing system. The corresponding fall distances varied from 600–1000 m. Fig. 7 shows the predicted SLCP, seedline and fallout area of crystals for an aircraft flare release at 4000 m into a cloud with average LWC = 0.10 g m⁻³ at 1800 UTC 5 February 1986.

3) PROCEDURES FOR AIRBORNE ACETONE GENERATORS

The targeting calculations for experiments which utilized airborne acetone generators were nearly identical to those for flare or CO₂ releases, but the methods to calculate the SLCP and fallout area differed. The primary difference between the two seeding techniques was that the flares and CO₂ produced a deep vertical curtain while airborne generators produced narrow continuous plumes. The target crystal for airborne generator releases was initiated at the altitude of the seeder aircraft. The method to determine the spread of the seeding effect took into account the variation in activation time of individual aerosols.

Various chemical solutions have been developed for use in airborne aerosol generators. The solution used in SCPP generators, a 3% AGINH₄I acetone mixture with 30 mole% NH₄ClO₄, has been studied extensively in the isothermal cloud chamber at the Colorado State University Aerosol and Cloud Simulation Laboratory (DeMott et al. 1983). DeMott et al. found this compound to have a high yield at warm (-6° to -10°C) temperatures and function primarily by contact nucleation. They observed 50% of all nucleation events within 5 min after introduction of the nuclei into the chamber and 90% within 20 min.

DeMott et al. data concerning the nucleation rate

¹ The flares were manufactured by Nuclei Engineering Inc.

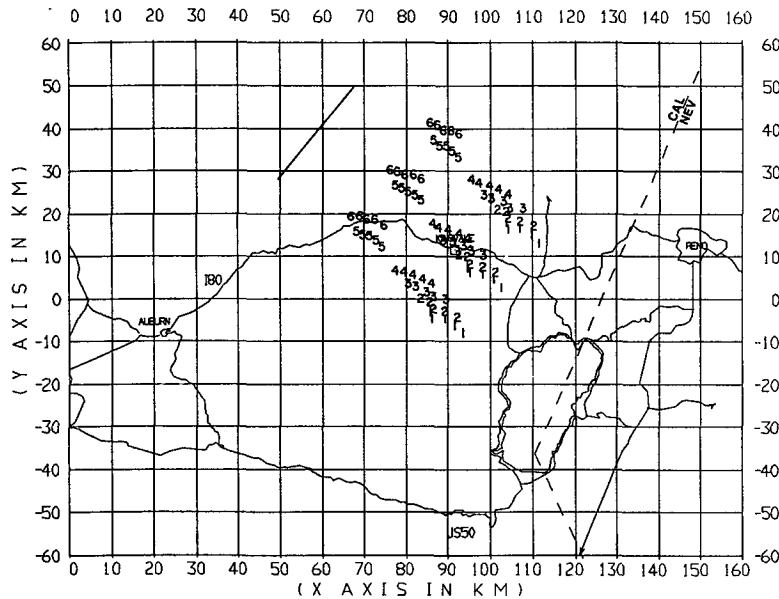


FIG. 7. Calculated seedline and fallout area of crystals for an aircraft flare release at 4000 m into a cloud with average LWC = 0.10 g m⁻³ on 5 February 1986 at 1800 UTC. The numbers 1-6 represent particles that originated at 200 m elevation intervals at the top (1) through bottom (6) of the 1 km deep curtain produced by the dropping flares. Each number appears five times representing the fallout location of particles originating at the same location, but falling with different fall velocities (see Eq. 7).

of AgINH₄I were incorporated into the targeting calculations. The assumption was made that nucleation would continue downwind of the release point with half of all nucleation events occurring within the initial 5 min. The SLCP was calculated so that crystals nucleated within the first 5 min after release fell upwind of the target and crystals nucleated later fell downwind. The calculation of the SLCP proceeded exactly as described in subsection 3c(2), except that a 5 min delay time prior to nucleation of the target crystal was allowed. The fallout area was predicted by calculating the fallout trajectories of groups of crystals nucleating 0, 5, 10, 15 and 20 min downwind of the seedline. The same fallspeed parameterization described in subsection 3c(2) was used for crystals within each group. This scheme appeared adequate based on preliminary observations of seeding effects as reported by Deshler and Reynolds (1987).

4. Evaluation studies

An important emphasis of SCPP research was to evaluate the utility of the targeting scheme in operations by comparing the calculations with field measurements. In this section, three studies are presented which compare 1) the diagnosed wind fields (*u* and *v*) with aircraft measurements; 2) predicted ice particle growth rates and habits with those measured by aircraft in seeded cloud regions; and 3) radar echo evolution within seeded cloud regions with predicted particle trajectories.

a. Comparison of calculated and measured winds

Comparisons of calculated wind fields with those measured by aircraft were made for seven fixed target experiments during the 1985/86 winter season. The comparison was limited to the region of the atmosphere bounded by the aircraft flight (primarily within region A of Fig. 3). In each case, soundings that would have been used operationally were used to initialize the targeting model. The aircraft flight pattern was the same in each case. After performing a climbout sounding over the valley, the aircraft proceeded eastward, descending from 5000 to 4000 m. The aircraft crossed the crestline, then reversed course and proceeded westward, descending along the MOCA toward the valley. The final leg consisted of a climb over the foothills to the seeding altitude. This pattern completely encircled and penetrated the region of the cloud system influenced by seeding. The measured *u* and *v* wind components along this track were analyzed and graphically subtracted from calculated *u*- and *v*-component wind fields. Huggins et al. (1986) describe each comparison study in detail. Examples are presented here which demonstrate the important results.

Figures 8a-c show calculated (solid) and measured (dashed) *u*- and *v*-components of the wind during two fixed target experiments. The error fields, determined by graphical subtraction, are shown in Figs. 8d-f. Figures 8a, and d demonstrate important characteristics of the calculated *u*-component fields. In nearly all ex-

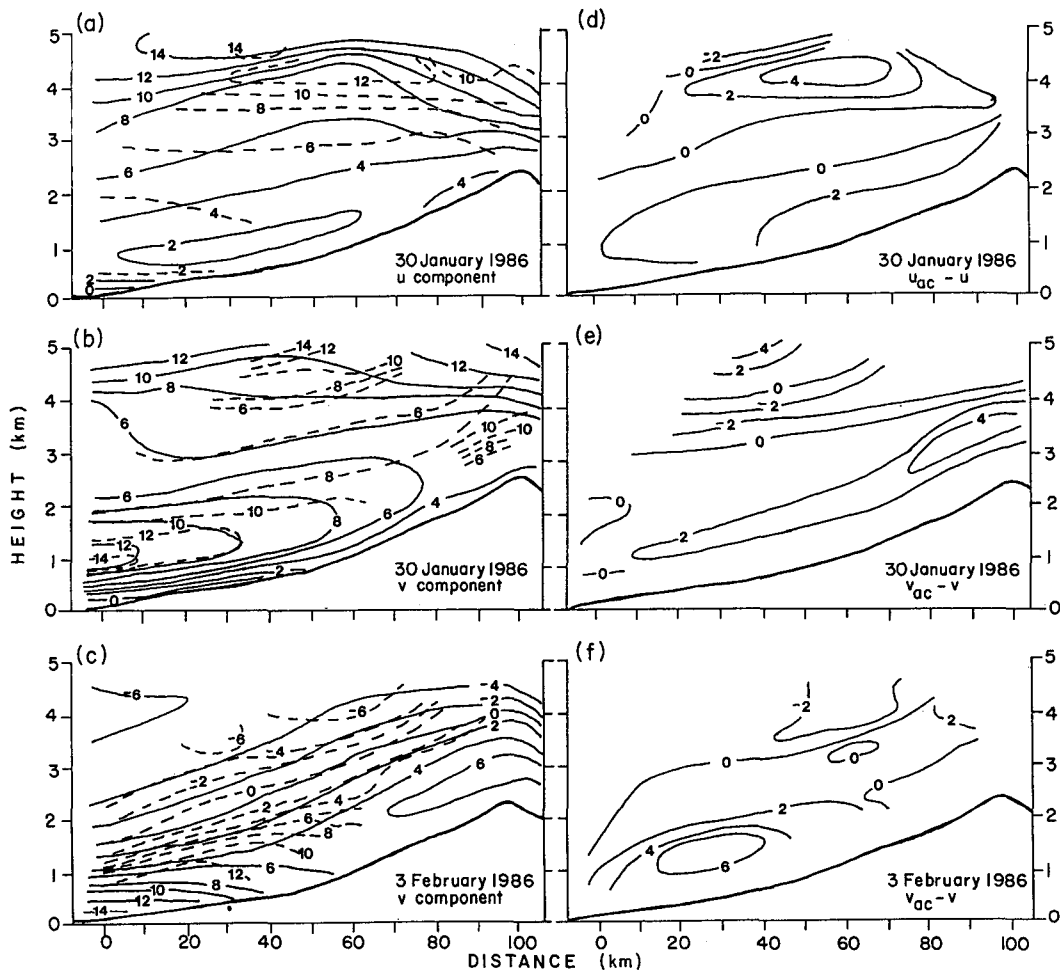


FIG. 8. (a) Calculated (solid) and aircraft measured (dashed) u -component of the wind (m s^{-1}) on 30 January 1986; (b) as in a, but for v -component; (c) as in a, but for v -component on 3 February; (d) graphical subtraction (measured-calculated) of fields in panel a; (e) graphical subtraction of fields in panel b; (f) graphical subtraction of fields in panel c.

periments, errors in the u -component were less than 4 m s^{-1} throughout the 100 km domain from the base of the Sierra Nevada to the crestline. In most locations within this region, errors were $< 2 \text{ m s}^{-1}$. The primary exception to the quoted error values occurred in regions of strong vertical shear. The magnitude of the velocities within shear zones was normally reproduced closely, but the location of the shear zone was sometimes displaced upward or downward a few hundred meters in altitude. This displacement typically resulted in a narrow region of larger errors. Such a region is evident between 4 and 5 km altitude in Figs. 8a and d. The largest error in any experiment ($\sim 10 \text{ m s}^{-1}$) occurred within such a shear zone. In almost all cases, these zones of higher shear were above the seeding altitude and had no effect on the calculated particle trajectories.

The v -component of the wind typically was maximum within the core of the barrier jet (Parish 1982) approximately 1 km above the lower Sierra Nevada foothills. Figure 8b shows a typical barrier jet profile

measured by the aircraft and calculated for targeting. Figure 8e shows the error analysis of these fields. Under conditions when the barrier jet decreased linearly toward the barrier crest, errors in the calculated v -component were minimized. This was the case on 30 January, where errors were generally $2\text{--}4 \text{ m s}^{-1}$ throughout the seeded volume. Contrast this profile with that measured on 3 February 1986 (Fig. 8c). In this case, the jet extended further into the lower foothills than would have been anticipated based on a linear interpolation between the Sheridan and Kingvale soundings. As a result, a narrow core of larger errors (Fig. 8f) was located over the lower foothills. Errors in the v -component were generally highest in this region.

The target was designed so that the sampling site, Kingvale, would be at the center of the area on the ground where seeding effects should have occurred. However, errors in the calculated wind field would shift the center of the predicted fallout area away from the target. An estimate of the magnitude of this shift was

computed for each of the fixed target experiments of 1985–86 by integrating the errors along the entire particle trajectories. The error in the center of the fallout area due to errors in the wind fields was almost always within 10 km of the Kingvale site and often within 5 km. This shift generally, but not always, left Kingvale within the expected area of effect.

b. Ice particle growth rates

Ice particle growth rates used in targeting were based on the laboratory measurements of Ryan et al. (1976) and Fukuta and Wang (1984). These experiments were conducted under water saturated conditions. In the Ryan et al. experiments, water saturation was maintained by growing crystals in an environment with liquid water contents near 3 g m^{-3} . These diffusional growth rates therefore represent maximums expected in real atmospheric conditions.

During SCPP, ice particles created by seeding have been observed in a number of experiments (e.g., Stewart and Marwitz 1982b; Martner 1986; Deshler and Reynolds 1987). Natural conditions in the vicinity of seeded regions have varied substantially. This natural variability has had a substantial effect on the identification of seeding effects. Martner (1986) found that only 25% of the seedlines penetrated by aircraft showed unambiguous seeding effects. In the remaining 75%, seeding effects did not appear either because highly variable and large ice particle concentrations already existed naturally or large droplets masked the signal on the optical array probes (Rauber and Heggli 1988).

When seeding effects were observed in the orographic cloud systems, somewhat consistent information emerged. With few important exceptions, particle growth rates were found to be consistent over a broad temperature range. Figure 9 shows a plot of observed

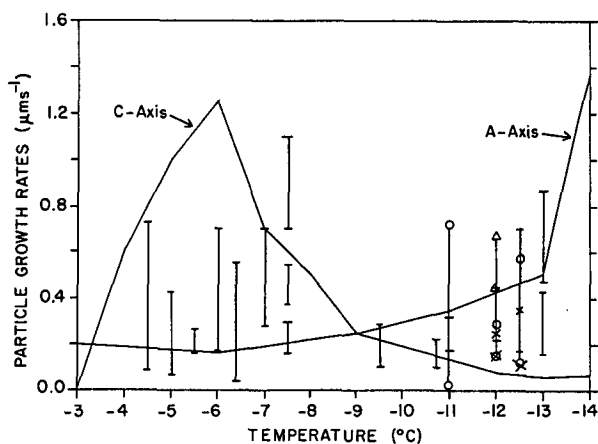


FIG. 9. (Solid lines) Variation of crystal axial growth rates with temperature from Ryan et al. (1976) experiments. (Line segments) Estimated crystal growth rates based on optical array probe images collected during seedline penetrations (see text). Coincident line segments are indicated by different symbols.

particle growth rates in seeded regions derived from cloud physics aircraft data collected at various temperature levels. The particle growth rates were determined by measuring sizes of particles associated with seeding from optical array probe images at the time of seedline penetration and dividing these values by the time elapsed between the release of the seeding material and the observation. Particles associated with seeding were identified by comparing particle spectra measured during the seedline penetration with those directly outside the region of seeding effects. These data are also tabulated in Table 3. The table also describes ambient cloud conditions and other pertinent information associated with each observation. The diffusional growth rate curves of Ryan et al. (1976) are also shown in Fig. 9.

Although scatter exists in the observations, the observed growth rates in the seeded regions of clouds generally fell below the rates measured in the laboratory. With one exception, no enhanced growth was observed along the *c*-axis between -4.5° and -7.5°C . The exception occurred during one seedline penetration on 5 February 1983 where needlelike habits were observed. In all other cases, small thick columns, hexagonal plates, or small irregular particles were observed. These habits are characteristic of sub-water saturated conditions. The high ice particle concentrations, reductions in supercooled water observed in plume penetrations, and consistent particle habits and slow growth rates all suggest that sub-water saturated conditions existed locally in plumes due to overseeding. It is interesting to note that supercooled liquid was observed on the seedline during the case when larger needles were observed. In the temperature range $< -8^\circ\text{C}$, growth rates and habits more closely matched the laboratory measurements. It is important to point out that the seeding agent in several cases was AgI. Small particles were observed on the seedline through 40 and 81 min, respectively, on 18 and 22 December 1986. These small particles may indicate slow growth rates, but, more likely were due to continued nucleation well downwind of the release point.

According to Heymsfield (1987), preferred mechanisms of growth occur after initial diffusional growth depending on the habit of the particle. He found that particles with small cross-sectional area grow by accretion much more efficiently than by aggregation. In contrast, particles with large cross-sectional areas, such as needles growing at -6°C , or dendrites growing at -15°C , grow efficiently by aggregation. Direct observations within seeded plumes suggested that the primary growth mechanism in shallow orographic cloud systems seeded in SCPP during the later period of crystal growth was accretion. Aggregation was rarely observed. Heymsfield's results indicate that for liquid water contents normally present in these cloud types ($0.05\text{--}0.20 \text{ g m}^{-3}$), maximum dimensions reached before impact would be $500\text{--}800 \mu\text{m}$ and terminal ve-

TABLE 3. Comparison of observed and predicted particle growth rates during seedline penetrations. The seeding agent for each date is designated CO₂ (asterisk) or AgI (plus).

Date	Time after seeding (min)	Typical particle size (μm)	Particle habits	Temperature at seeder aircraft altitude ($^{\circ}\text{C}$)	Predicted growth rate at seeder temperature ($\mu\text{m s}^{-1}$)	Predicted major axis at seeder temperature	Temperature at Kings-Air sampling altitude ($^{\circ}\text{C}$)	Predicted growth rate at sampling temperature ($\mu\text{m s}^{-1}$)	Predicted major axis at sampling temperature	Observed growth rate ($\mu\text{m s}^{-1}$)	Comments on ambient cloud conditions
02 Feb. 80*	19.0	250-500	Plates, some branching observed	-13.0	0.92	a	-12.0	0.54	a	0.22-0.44	LWC: <0.1 g m ⁻³ (generally low), Natural ice particle conc (2DC) <1 L ⁻¹
03 Mar. 80*	31.0	300-500	Regular thick columns	-7.0	0.62	c	-5.5	1.04	c	0.16-0.27	LWC: 0.0-0.2 g m ⁻³ (generally low), 2DC: <5 L ⁻¹
05 Feb. 83*	9.5	400-600	Columns or needles	-11.0	0.33	a	-7.5	0.52	c	0.70-1.10	LWC: 0.0-0.2 g m ⁻³ (present in plume), 2DC: <10 L ⁻¹
05 Feb. 83*	9.0	200-300	Thick columns or plates?	-11.0	0.33	a	-7.5	0.52	c	0.37-0.55	LWC: 0.0-0.2 g m ⁻³ (in pockets, mostly near 0), 2DC: <1 L ⁻¹
05 Feb. 83*	28.0	300-500	Rimed	-11.0	0.33	a	-7.5	0.52	c	0.18-0.30	LWC: 0.0-0.2 g m ⁻³ (mostly near zero), 2DC: <10 L ⁻¹
24 Feb. 84*	12.0	200-500	Rimed irreg. columns and needles	-9.0	0.25	a	-7.0	0.62	c	0.28-0.70	LWC: 0.1-0.5 g m ⁻³ (highest in cells), 2DC: <5 L ⁻¹
26 Jan. 85*	23.0	200-400	Plates	-14.0	1.42	a	-12.0	0.54	a	0.15-0.29	LWC: 0.0-0.05 g m ⁻³ (almost all zero), 2DC: <5 L ⁻¹
26 Jan. 85*	33.0	300-500	Plates	-14.0	1.42	a	-12.0	0.54	a	0.15-0.25	LWC: 0.0 g m ⁻³ , 2DC: <5 L ⁻¹
28 Jan. 85*	9.5	100-400	Plates	-15.0	1.83	a	-12.5	0.73	a	0.17-0.70	LWC: 0.05-0.10 g m ⁻³ , 2DC: <5 L ⁻¹
28 Jan. 85*	14.5	100-500	Plates	-15.0	1.83	a	-12.5	0.73	a	0.12-0.57	LWC: 0.05-0.10 g m ⁻³ (pockets to 0.25), 2DC: <5 L ⁻¹
28 Jan. 85*	23.5	150-500	Plates	-15.0	1.83	a	-12.5	0.73	a	0.11-0.35	LWC: 0.05-0.10 g m ⁻³ , 2DC: <5 L ⁻¹
02 Feb. 85*	3.5	100-200	Plates	-15.0	1.83	a	-13.0	0.92	a	0.47-0.95	LWC: 0.05-0.10 g m ⁻³ , 2DC: <15 L ⁻¹
02 Feb. 85*	15.5	300-400	Plates	-15.0	1.83	a	-13.0	0.92	a	0.32-0.43	LWC: 0.05-0.10 g m ⁻³ , 2DC: <15 L ⁻¹
03 Feb. 86*	7.5	200-300	Rimed particles?	-9.5	0.27	a	-12.0	0.54	a	0.44-0.67	LWC: 0.1 g m ⁻³ , 2DC: <45 L ⁻¹
03 Feb. 86*	17.0	200-400	Rimed particles?	-9.5	0.27	a	-9.5	0.27	a	0.20-0.39	LWC: 0.0 g m ⁻³ , 2DC: 80 L ⁻¹
03 Feb. 86*	25.0	300-500	Rimed particles?	-9.5	0.27	a	-10.7	0.32	a	0.20-0.33	LWC: 0.0 g m ⁻³ , 2DC: 40 L ⁻¹
03 Feb. 86*	36.0	400-700	Rimed particles?	-9.5	0.27	a	-11.0	0.33	a	0.18-0.32	LWC: 0.05 g m ⁻³ , 2DC: 30 L ⁻¹
18 Dec. 86*	9.5	100-400	Columns	-6.0	1.26	c	-6.0	1.26	c	0.18-0.70	LWC: 0.1-0.4 g m ⁻³ , 2DC: 1-50 L ⁻¹
18 Dec. 86*	40.0	200-1750	Rimed particles	-6.0	1.26	c	-4.5	0.80	c	0.08-0.73	LWC: 0.1-0.4 g m ⁻³ , 2DC: 1-50 L ⁻¹
22 Dec. 86*	28.0	100-700	Irregular	-5.0	1.00	c	-5.0	1.00	c	0.06-0.42	LWC: 0.05-0.20 g m ⁻³ , 2DC: 25-50 L ⁻¹
22 Dec. 86*	42.0	100-1400	Irregular	-5.0	1.00	c	-6.8	0.83	c	0.04-0.55	LWC: 0.05-0.20 g m ⁻³ , 2DC: 25-50 L ⁻¹
22 Dec. 86*	81.0	100-3500	Irregular	-5.0	1.00	c	-11.0	0.40	a	0.02-0.72	LWC: 0.05-0.20 g m ⁻³ , 2DC: 15-25 L ⁻¹

locities will approach or exceed 1 m s^{-1} due to the small cross-sectional area of the crystals.

In the targeting calculations, the diffusional growth rate and habit parameterizations appear to correspond well with observations in the temperature region from -8° to -13°C where slow diffusional growth rates were observed both experimentally and in the laboratory. The riming parameterization, based on the Heymsfield (1982) and Heymsfield and Pflaum (1985) model, produced particles with fall velocities within ranges estimated by Heymsfield (1987) for temperatures $< -8^\circ\text{C}$ and typical supercooled water contents encountered in SCPP experiments. However, at temperatures $> -8^\circ\text{C}$ sub-water saturated conditions within seeded regions were found to limit growth so that particles retained habits more similar to that observed between -7° and -12°C . As a result, the parameterization overestimated particle growth rate at temperatures near -6°C . However, the fall velocity of these particles was actually underestimated because the assumed particle habit (needles) was incorrect, except in one case. Particles with needlelike habits have reduced fall velocities due to their larger cross-sectional area (see Fig. 5).

c. Radar echo evolution within seeded cloud regions

Storm systems over the Sierra Nevada generally contain sufficient numbers of natural large ice particles so that seeding effects cannot be discerned within natural background reflectivity measurements made with radar. However, in some systems, particularly those characterized by weak convective regions (Huggins and Rodi 1985), seeding effects have been observed with radar. In this section the 24 February 1984 storm system is discussed. This storm is one of the three best storms when meteorological conditions permitted comparison of radar measurements within seeded regions with calculated particle trajectories. The other two storms where the radar has been used to observe seeding effects are discussed by Deshler and Reynolds (1987).

On 24 February, the clouds had the appearance of stratocumulus during most of the experimental period. Some convective cloud tops extended above 3 km. Seeding was done with CO_2 pellets near cloud top. Seeding effects, documented previously by Martner (1986), were noted in the aircraft data downwind of two seeding lines.

Optical array probe images showed the largest particles, at 12 min after seeding, were on the upwind edge of the curtain, and consisted of 400–500 μm graupel, or rimed columns and needles of similar size. If these particles were nucleated at the time of seeding they grew at a rate of $\sim 0.6 \mu\text{m s}^{-1}$. However, most particles were smaller than 0.4 mm. The diffusional/accretional model of Cooper and Lawson (1984) predicted that a particle growing at -8°C in 1 g m^{-3} liquid could reach 500 μm diameter in about 15 min and 1 mm in 24 min. The particles detected by the aircraft at compa-

table times were smaller ($\sim 300 \mu\text{m}$ at 15 min), probably due to liquid water content being less than 1 g m^{-3} within the seeded ice particle curtain.

Using the techniques of Huggins and Rodi (1985), the radar data for 24 February were examined for seeding effects. Several clear examples of radar echoes developing downwind of seeding were found. The development of these echoes closely resembled the radar seeding signatures found by Huggins and Rodi in weak convective clouds seeded with CO_2 . In one case, a radar echo formed about 10 min downwind of a region seeded at 2040:30 UTC. The first echo was detected between 2.15 and 2.90 km (-5° to -10°C) and had a maximum intensity of 4 dBZ.

The trajectory calculations for a crystal initiated on the seedline at -7°C was compared to the seeded echo development. The predicted fallout location was 33 min downwind at a point 16 km from the seed point. Using a value of 0.1 g m^{-3} for liquid water content, the predicted crystal was a rimed column that attained a major axis of 1.04 mm.

A time–height analysis of maximum dBZ for the seeded cell is shown in Fig. 10. The echo increased slowly in intensity to 10 dBZ by 2059 UTC ($t_0 + 19$). This was in contrast to typical Huggins and Rodi (1985) cases where aggregation resulted in a very rapid increase of reflectivity after echo formation. The 10 dBZ contour intercepted the surface at about 2113 UTC ($t_0 + 33$). A plot of the predicted crystal trajectory on the same figure shows similarity to the 10 dBZ contour slope. The crystal was computed to impact the surface at a point 33 min downwind of the SLCP, identical to the radar echo 10 dBZ contour. The radar showed weaker echo impacted the surface at 2108 UTC from a region below the SLCP, possibly as low as 2.0 km

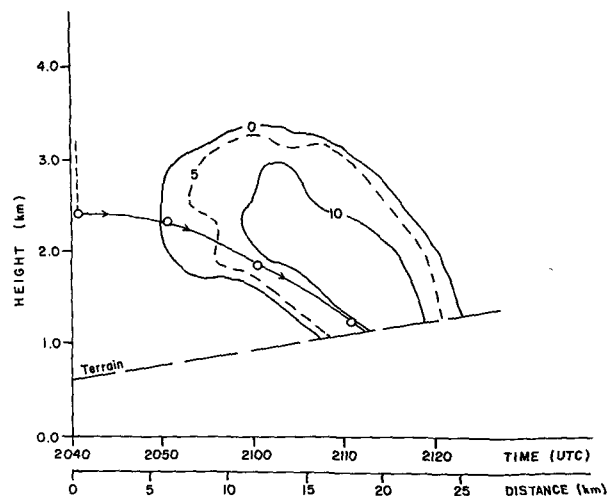


FIG. 10. Time-height development of radar echo (dBZ) in a seeded cloud on 24 February 1984 compared to calculated trajectory (solid line with arrows) for a rimed column initiated at -7°C . Vertical dashed line represents seeding curtain at t_0 .

($\sim -5^{\circ}\text{C}$). It also shows crystals from the center of the 10 dBZ region probably initiated around 2.8 km (-9.5°C).

At the point of echo formation (4 dBZ), the predicted crystal was a $554\ \mu\text{m}$ column with a fallspeed of $0.55\ \text{m s}^{-1}$. At the point where a 10 dBZ echo was first observed ($t_0 + 19$) the predicted crystal was a rimed column with a major axis of $1004\ \mu\text{m}$ and a fallspeed of $1.1\ \text{m s}^{-1}$. The slope of the 10 dBZ echo contour implied a particle fallspeed of $1.25\ \text{m s}^{-1}$. The final calculated crystal fallspeed was $1.13\ \text{m s}^{-1}$.

The speed of the radar echo was measured at $10.2\ \text{m s}^{-1}$ between 2055 and 2111 UTC. At the point where the 10 dBZ contour reached the surface, the echo was 20.8 km downwind of the seeding location. By comparison the calculated trajectory terminated 16 km downwind of the SLCP. The crystal moved at an average speed of $8.1\ \text{m s}^{-1}$. An x - z plot of radar echo and the calculated crystal trajectory illustrate this difference in Fig. 11. Points of equivalent times of the radar echo path and crystal trajectory are shown.

In general, there was good agreement between radar echo evolution and predictions for fallout time of a crystal originating at the SLCP at -7°C . The crystal was predicted to fall out in 33 min, nearly identical to the radar results. However, the downwind distance traveled differed by 5 km. This may have been due to errors in the calculated wind field (see sec. 4a), since mean echo motion was observed to be approximately $2\ \text{m s}^{-1}$ faster than the mean predicted crystal horizontal velocity.

6. Summary and conclusions

The diagnostic method for targeting during airborne seeding experiments of the Sierra Cooperative Pilot Project was described in this paper. During aircraft seeding operations, this technique was used operationally to direct aircraft to the appropriate seeding location in the cloud in order to target effects to a specific ground location. The area of effect on the ground was also estimated. The methods used were data-interactive, so

that the latest possible information concerning the local wind fields and cloud liquid water content could be incorporated into the targeting calculations. The parameterizations were simple, designed for operational expediency. The total time required to perform the targeting calculations and direct the aircraft to the seeding location was usually under 3 min.

Three evaluations of the targeting technique were presented. These studies include comparisons of 1) predicted wind fields with those measured by aircraft; 2) ice particle growth rates within seeded cloud regions with predicted growth rates; and 3) radar echo evolution within seeded cloud regions with predicted particle trajectories.

The diagnosed wind fields over the Sierra Nevada were found to generally correspond to aircraft measurements of wind speed and direction within the lower atmosphere ($<5000\ \text{m}$) upwind of the crestline. Errors in the u - and v -components of the wind were generally $<4\ \text{m s}^{-1}$ over the 100 km domain upwind of the crest. Exceptions were noted in regions of strong vertical shear and/or when the barrier jet core extended far into the foothills. In these cases, narrow regions of more significant errors (4 – $10\ \text{m s}^{-1}$) were observed. These regions of large error were generally above (shear) or west (barrier jet) of the primary region where seeding was conducted. The displacement of predicted fallout locations due to misrepresentation of the wind fields within the region affected by seeding was less than 10 km from the target in nearly all cases, and often less than 5 km.

Comparison of predicted ice particle habits and growth rates with those measured within seeded regions of storms were made during 11 storm systems. Ice particles were sampled by aircraft 4–81 min after seeding. Particle habits and growth rates used in the targeting parameterization generally agreed with measurements taken in the temperature range -8° to -13°C . At warmer temperatures, particle growth rates were generally overestimated. Habits were typically thick columns, plates or rimed particles rather than the expected needle. The reason for the discrepancy appeared to be

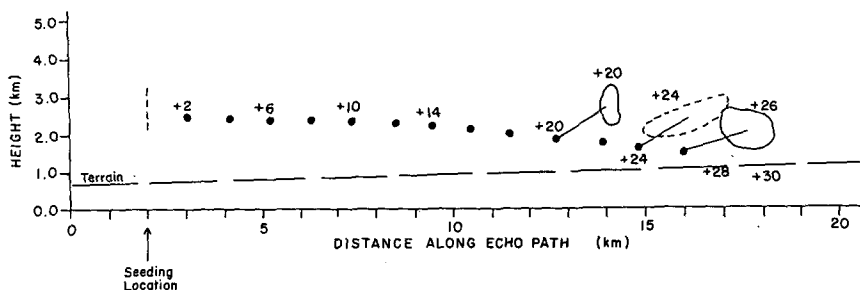


FIG. 11. Comparison of calculated crystal trajectory and radar echo development in the X - Z plane. Dots connect calculated crystal position and echo at equivalent times. The radar echo contour represents 5 dBZ. Vertical dashed line represents seeding curtain.

associated with the absence of water saturated conditions locally on the seedline. The high ice particle concentrations found on the seedline suggested that sub-water saturated conditions may have been due to over-seeding. It appeared from the data that sub-water saturated conditions prevented the development of needlelike habits at these temperatures.

A case study comparing radar echo evolution in seeded cloud regions with predicted particle trajectories was presented. In general, good agreement between radar echo evolution and predicted particle trajectories was obtained. The predicted falltime was nearly identical to the radar results, but the predicted fallout location differed by 5 km.

In most cloud seeding applications, target areas are of limited extent and the opportunities for cloud modification are limited in duration. In the Sierra Nevada region, these problems are compounded by the rapid evolution and complex structure of many storm systems. To conduct successful seeding operations, it is important that the best estimate of the appropriate place to seed is available in a short time frame. The methods described in this paper represent one attempt to accomplish this task. As targeting methods continue to be developed and refined, better evaluations of the effects of weather modification should become available. With refined targeting techniques, the role of weather modification in the management of water resources can be more effectively assessed.

Acknowledgments. This work was sponsored by the Department of Interior, Bureau of Reclamation under Contracts 9-07-85-V0021, 4-CR-81-03860 and 7-07-83-V0008. The authors would like to thank all SCPP participants for their contributions to this paper. Particular thanks to the staff of the University of Wyoming, who provided data and expertise associated with the King Air. A special acknowledgement is due to the staff of Electronic Techniques, Inc., particularly Ms. Carol Wilcox, who drafted the figures and typed the manuscript, and Mr. Arunas Kuciauskas, who developed software to display radar data and targeting calculations.

REFERENCES

- Anthes, R. A., and T. T. Warner, 1978: Development of hydrodynamic models suitable for air pollution and other mesometeorological studies. *Mon. Wea. Rev.*, **106**, 1045-1078.
- Brown, S. R., 1970: Terminal Velocities of Ice Crystals. Atmos. Sci. Paper No. 170, Colorado State University, Fort Collins, Colorado 80523.
- Browning, K. A., and G. A. Monk, 1982: A simple model for the synoptic analysis of cold fronts. *Quart. J. Roy. Meteor. Soc.*, **101**, 893-900.
- Bureau of Reclamation, 1985: Design of a randomized exploratory fixed target experiment on widespread winter orographic clouds. Bureau of Reclamation, Div. of Atmos. Res. Research, D-1200, Box 25007, Denver, CO 80225, 52 pp.
- Clark, T. L., 1977: A small scale dynamic model using a terrain following coordinate transformation. *J. Comput. Phys.*, **24**, 186-215.
- Cooper, W. A., and R. P. Lawson, 1984: Physical interpretation of results from the HIPLEX-1 experiment. *J. Climate Appl. Meteor.*, **23**, 523-540.
- Cornford, S. G., 1965: Fallspeeds of precipitation elements. *Quart. J. Roy. Meteor. Soc.*, **91**, 91-94.
- Davis, C. I., 1974: Ice nucleating characteristics of various AgI aerosols. Ph.D. dissertation, University of Wyoming, 259 pp.
- DeMott, P. J., W. G. Finnegan and L. O. Grant, 1983: An application of chemical kinetic theory and methodology to characterize the ice nucleating properties of aerosols used in weather modification. *J. Climate Appl. Meteor.*, **22**, 1190-1203.
- Deshler, T., and D. W. Reynolds, 1987: The evolution of artificially nucleated ice crystals in shallow orographic winter clouds: Two case studies. *11th Conf. on Weather Modification*, Edmonton, Amer. Meteor. Soc., 34-39.
- Elliott, R. D., 1981: A seeding effects targeting model. *Preprints of Eighth Conf. on Inadvertent & Planned Weather Modification*, Reno, Amer. Meteor. Soc., 28-29.
- , and J. O. Rhea, 1984: Comparison of observed and predicted model winds over an orographic barrier. *Proc. Ninth Weather Modif. Conf.*, May 21-23, Park City, Amer. Meteor. Soc., 83-84.
- Flueck, J. A., 1982: Comparative experimentation: Some principles and prescriptions. *Teaching of Statistics and Statistical Consulting*, J. Rustagi and D. Wolfe, Eds., Academic Press, Inc., 433-463.
- Fukuta N., and A. S. Wang, 1984: The studies of growth rates of ice crystal at different temperature and ice supersaturation. *Proc. Ninth Int. Conf. Cloud Physics*, Tallinn, Estonia, USSR. 183-186.
- Gordon, G. L., and J. D. Marwitz, 1986: Hydrometeor evolution in rainbands over the California valley. *J. Atmos. Sci.*, **43**, 1087-1100.
- Hallett, J., and B. J. Mason, 1958: The influence of temperature and supersaturation on the habit of ice crystals grown from the vapor. *Proc. Roy. Soc. London*, **A247**, 440-453.
- Heggl, M., 1986: A ground based approach used to determine cloud seeding opportunity. *Tenth Conf. on Weather Modif.*, Arlington, Amer. Meteor. Soc., 64-67.
- , and D. W. Reynolds, 1985: Radiometric observations of supercooled liquid water within a split front over the Sierra Nevada. *J. Climate Appl. Meteor.*, **24**, 1258-61.
- Heggl, M. F., R. M. Rauber and J. B. Snider, 1987: Field evaluation of a dual-channel microwave radiometer designed for measurements of integrated water vapor and cloud liquid water in the atmosphere. *J. Atmos. Oceanic Technol.*, **4**, 204-213.
- Heymsfield, A., 1982: A comparative study of the rates of development of potential hail embryos in the High Plains storms. *J. Atmos. Sci.*, **39**, 2867-2897.
- , 1987: Aggregates as embryos in seeded clouds. *Precipitation Enhancement—A Scientific Challenge*. Meteor. Monogr. No. 21 and No. 43, Amer. Meteor. Soc., 33-41.
- , and J. C. Pflaum, 1985: A quantitative assessment of the accuracy of techniques for calculating graupel growth. *J. Atmos. Sci.*, **42**, 2264-2274.
- Hobbs, P. V., 1978: Organization and structure of clouds and precipitation on the mesoscale and microscale in cyclonic storms. *Rev. Geophys. Space Phys.*, **16**, 741-755.
- Huggins, A. W., and A. R. Rodi, 1985: Physical response of convective clouds over the Sierra Nevada to seeding with dry ice. *J. Climate Appl. Meteor.*, **24**, 1082-1098.
- , R. M. Rauber, T. W. Lee, A. P. Kuciauskas, G. L. Hemmer and C. J. Wilcox, 1986: SCPP Meteorological and Statistical Support, Interim Progress Rep. 1985-86. [Available from Bureau of Reclamation, Division of Atmospheric Resources Research, D-1220, Denver Federal Center, Denver, CO 80225.]
- Humphries, J. H., 1985: Applications of an airborne optical array probe for ground-based microphysical observations. *J. Atmos. Oceanic Technol.*, **2**, 253-259.
- Kajikawa, M., 1971: A model experimental study on the falling velocity of ice crystals. *J. Meteor. Soc. Japan*, **49**, 367-375.

- King, W. D., 1984: Seeding stratiform clouds: The effects of cloud parameters on aiming. *J. Climate Appl. Meteor.*, **23**, 1265–1272.
- Kobayashi, T., 1961: The growth of snow crystals at low supersaturations. *Phil. Mag.*, **6**, 1363–1370.
- List, R., and R. S. Schemanauer, 1971: Free-fall behavior of planar snow crystals, conical graupel and small hail. *J. Atmos. Sci.*, **28**, 110–115.
- Locatelli, J. D., and P. V. Hobbs, 1974: Fallspeeds and masses of solid precipitation particles. *J. Geophys. Res.*, **79**, **15**, 2185–2197.
- Magono, C., and C. W. Lee, 1966: Meteorological classification of natural snow crystals. *J. Fac. Sci. Hokkaido Univ. Ser. 7*, **2**, 321–362.
- Martner, B. E., 1986: Microphysical seeding effects in nonconvective clouds over the Sierra Nevada. *Tenth Conf. on Weather Modification*, Arlington, Amer. Meteor. Soc., 30–33.
- Marwitz, J. D., 1987: Deep orographic storms over the Sierra Nevada. Part I: Thermodynamic and kinematic structure. *J. Atmos. Sci.*, **44**, 159–173.
- Nakaya, U., 1954: *Snow Crystals: Natural and Artificial*. Harvard University Press, 510 pp.
- Parish, T. R., 1982: Barrier winds along the Sierra Nevada mountains. *J. Appl. Meteor.*, **21**, 925–930.
- Prasad, N., 1986: Precipitation development in seeded clouds over the Sierra Nevada. Rep. #AS152, Dept. of Atmos. Sci., University of Wyoming, Laramie, WY 82071. Contract 2-07-81-V0256, Bureau of Reclamation.
- Rasmussen, R. M., P. Smolarkiewicz, W. D. Hall and T. Clark, 1988: Comparison of orographic cloud and precipitation development of three different geographic locations using a 3-D nested grid model. *Tenth ICCP Conf. on Cloud Physics*, Bad Homburg, West Germany.
- Rauber, R. M., and M. F. Heggli, 1988: The influence of cloud droplets on the measurement of ice particle concentrations with a Particle Measuring Systems 2D-C optical array probe. *J. Atmos. Oceanic Technol.*, (in press.)
- Reinking, R. F., 1974: Cross-sectional areas of snow crystals and the accretion process. *Preprints Conf. Cloud Physics*, Tucson, Amer. Meteor. Soc., 185–190.
- , 1979: The onset and early growth of snow crystals by accretion of droplets. *J. Atmos. Sci.*, **36**, 870–881.
- Reynolds, D. W., and A. S. Dennis, 1996: A review of the Sierra Cooperative Pilot Project. *Bull. Amer. Meteor. Soc.*, **67**, 513–523.
- , and A. P. Kuciauskas, 1987: Remote and in-situ observations of Sierra Nevada winter mountain clouds: Relationships between mesoscale structure, precipitation and liquid water. *J. Climate and Appl. Meteor.*, **27**, 140–156.
- Rhea, J. O., and R. D. Elliott, 1986: A targeting computational framework for study and airborne seeding experiment use. *Tenth Conf. on Weather Modification*, Arlington, Amer. Meteor. Soc., 18–23.
- Rodi, A. R., A. S. Heymsfield and N. Prasad, 1985: Precipitation formation in dry ice seeding plumes. *Fourth WMO Conf. on Weather Modif.*, Honolulu, WMO, 71–76.
- Ryan, B. F., E. R. Wishart and D. E. Shaw, 1976: The growth rates and densities of ice crystals between -3°C and -21°C . *J. Atmos. Sci.*, **33**, 842–850.
- Smith, R. B., 1979: The influence of mountains on the atmosphere. *Advances in Geophysics*, Vol. 21, Academic Press, 87–127.
- Stewart, R. E., and J. D. Marwitz, 1982a: The downwind spread of an initially vertical column of particles in a sheared environment. *J. Appl. Meteor.*, **21**, 1191–1193.
- , and ———, 1982b: Microphysical effects of seeding wintertime stratiform clouds near the Sierra Nevada mountains. *J. Appl. Meteor.*, **21**, 874–880.
- Waight, K. T., III, 1984: A numerical study of the Sierra Nevada Barrier Jet. Atmospheric Science Paper No. 148, University of Wyoming, Laramie, WY.